DOI: ADD DOINUMBER HERE

An Innovative Strategy for Paraffin-based Fuels Reinforcement: Part I, Mechanical and Pre-Burning Characterization

Riccardo Bisin[⋆†]*, Christian Paravan*[⋆]*, Sebastiano Alberti*[⋆] *and Luciano Galfetti*[⋆]
[⋆]*Politecnico di Milano, Aerospace Science and Technology Dept.,*
Space Propulsion Laboratory (SPLab)
34, via LaMasa, 20156, Milan, Italy
riccardo.bisin@polimi.it · christian.paravan@polimi.it · sebastiano.alberti@mail.polimi.it · luciano.galfetti@polimi.it
[†]Corresponding author

Abstract

Paraffin wax has been identified as a promising hybrid rocket fuel. Though attractive from the ballistics point of view, paraffin wax alone is a brittle material. In the present study, the reinforcement of paraffin is pursued through two different approaches: blending paraffin with a thermoplastic polymer and embedding 3D-printed cellular structures inside the pure paraffin. This is named *armored grain*. The most promising 3D-printed structure is selected and his structural behavior assessed. Mechanical properties of the fuel blends and the armored grains are characterized by compression tests.

1. Introduction

Hybrid rocket engines (HREs) are thermochemical propulsion systems in which the fuel and the oxidizer are stored in a different states of matter. Typically, the fuel is solid and the oxidizer is liquid. Thanks to their architecture, HREs offer several advantages over liquid and solid rocket engines: operating flexibility, high gravimetric specific impulse, intrinsic safety, reduced recurring costs, low environmental impact due to the absence of pollutant oxidizer employed in solid rocket motors [1]. However, the diffusion nature of the flame in HREs yields low regression rate (r_f), implying low thrust level and, hence, hampering the hybrid rocket technology implementation in operating systems. Paraffin-based fuels represent a low-cost and effective solution for the enhancement of r_f thanks to the entrainment phenomenon [2]. However, paraffin wax alone is a brittle, low strength material, unsuitable for withstanding loads associated to operations. Thus, the research activity on paraffin-based fuels aims at designing formulations featuring mechanical robustness and, at the same time, maintaining the capability of producing entrainment, which is promoted by low viscosity and low surface tension [2].

The enhancement of the mechanical properties of paraffin-based fuels is typically pursued by blending the wax with some reinforcing binder, like thermoplastic or thermosetting polymer. Nevertheless, this technique implies increased melt fuel viscosity hindering the entrainment and consequently the fuel regression rate [3]. Kobald et al. [4] investigated the effects on mechanical properties of different paraffins blended with stearic acid (SA), nanoclay and a not specified polymer. The tensile strength and maximum elongation at break of the blend with 10% polymer were respectively twice and three times the values of pure paraffin. On the contrary, a drop in the regression rate was experienced. Paraffin-polyethylene (PE) blends were studied by Kim et al. [5]. Mechanical assessment resulted in 24.8% tensile and 34% compression strength enhancement with respect to paraffin baseline for the 5% PE formulation. Same properties gained 42.4% and 42.2% respectively when 10% PE addition was considered. Styrene-Ethylene-Butylene-Styrene copolymer grafted with Maleic Anhydride (SEBS-MA) was studied at SPLab by Paravan et al. [6]. The tensile tests involved blends with SEBS-MA mass fraction from 0% to 30% at test speeds of 0.5 and 50 mm/min, at 8 °C and -19 °C. For weight percentage higher than 20-30% the samples featured a ductile behavior, resulting in the elongation at break enhancement. Galfetti et al. [7] investigated the stategy of pouring melted paraffin inside a polyurethane foam (PUF) structure. The randomness cell disposition of the foam led to anisotropic mechanical properties. Moreover, manufacturing process resulted complex and expensive.

The structural properties of paraffin grains can also be affected by the presence of aluminum particles. Ryu and co-workers [8] investigated mixtures with 10%, 20% and 30% nanosized aluminum (average particle size 100 nm) as well as with 5%, 10% and 15% of microsized aluminum (8 μm). The tensile and compression properties augmented thanks to the addition of both nano-Al and micro-Al.

Nowadays, additive manufacturing has been applied to hybrid rocket fuels. It enables a rapid and inexpensive production of conventional polymeric fuel grains characterized by complex geometries. The fused deposition modeling (FDM) and stereolithography (SLA) are the most used 3D-printing techniques. This manufacturing technique was investigated by Whitmore [9]. Conventional HTPB fuel grains produced via casting procedure were compared with Acrylonitrile Butadiene Styrene (ABS) 3D-printed fuels. Firing tests were performed with nitrous oxide as oxidizer. It was demonstrated that ABS fuel grains had a slightly reduced performance with respect to HTPB.
Another application of additive manufacturing consists in using printed structure as support for paraffin fuels. Armold et al. [10][11] investigated paraffin in a twisted honeycomb structure printed in acrylic. Their study focused on the enhancement of the regression rate by elevating the initial temperature of the fuel. The paraffin-acrylic honeycomb grains led to regression rate improvement without loss of combustion efficiency. Nevertheless, Armold did not conduct mechanical tests on the grains and no quantitative information on the mechanical properties is available in open literature.

In this framework, the efforts of Space Propulsion Laboratory (SPLab) of Politecnico di Milano are focused on investigating different strategies to enhance the structural properties of paraffin-based fuels. Studies have been carried out exploiting the effects of different strengthening agents. This paper aims at presenting a novel approach to reinforce the paraffin-based fuels, exploiting the use of additive manufacturing. Different 3D-printed cellular structures involving various printable materials have been investigated inspecting their structural behavior. The *armored grain*, a paraffin grain reinforced with a 3D-printed gyroid structure, is discussed in the present work.

2. Theory: Cellular Structures and Gyroid

The present study aims at reinforcing paraffin thanks to 3D-printed cellular structure embedded in the paraffin grain. Cellular or lattice materials are a connected network of struts. They have been deeply investigated by Ashby [12][13]. Cellular solids, also called cellular structures, include foam, honeycomb and regularly repeating lattice structures. The characteristic of a cellular material depends on three main factors.

- The properties of the bulk material.
- The topology (connectivity) and shape of the cell edges and faces.
- The relative density $\tilde{\rho}$, defined as the ratio between the density of the lattice ρ (i.e., the lattice mass divided by the occupied volume) and the density of the solid material ρ_s.

According to Ashby [12], the mechanical behavior of lattice material can be classified in bending- and stretch-dominated behavior. The former are compliant and prone to absorb energy when compressed. On the contrary, the latter are stiffer and stronger for a given mass. Examples of bending- and stretch-dominated structures are respectively foams and honeycombs. Bending-dominated structures are characterized by the bending deformation of the struts that compose the cell. In the stretch-dominated structures the cell edges stretch instead of bend.

Ashby proposed scaling laws to describe the mechanical behavior of cellular structure. The Young modulus E and the yield stress σ_y of the lattice structure are related to the properties of the bulk material (E_s, $\sigma_\mathrm{y,s}$) through the relative density $\tilde{\rho}$, i.e. the ratio between the density of the lattice ρ and the density of the solid material ρ_s. The Young modulus scales as

$$\frac{E}{E_\mathrm{s}} \propto \left(\frac{\rho}{\rho_\mathrm{s}}\right)^2 = \tilde{\rho}^{\,2} \quad \text{(bending-dominated behavior)} \tag{1}$$

$$\frac{E}{E_\mathrm{s}} \propto \left(\frac{\rho}{\rho_\mathrm{s}}\right) = \tilde{\rho} \quad \text{(stretch-dominated behavior)} \tag{2}$$

Concerning the yield stress, the scaling law can be written as

$$\frac{\sigma_\mathrm{y}}{E_\mathrm{s}} \propto \left(\frac{\rho}{\rho_\mathrm{s}}\right)^2 = \tilde{\rho}^{\,2} \tag{3}$$

Equation (3) is independent from the structure topology and it is valid under the assumption of slender struts that undergo buckling before yield.

The identification of the most suitable reinforcement structure for the paraffin fuels is based on the following considerations.

- **Open cell.** Open cell materials (e.g., foams) are preferred rather than closed ones (e.g, honeycomb) since the paraffin has to be inserted into the reinforcement structure by means of casting procedure (see Section 4.2) and the the structure itself has to be easily available during combustion.
- **Uniformity.** The lattice should feature uniform geometry and properties to prevent anisotropic combustion and mechanical behavior.
- **Volume usage.** Even though the structure is supposed to burn, the actual fuel shall be paraffin. A moderate volume of reinforcement should be selected to provide good mechanical properties.
- **Easy and fast prototyping.** The structure is required to be easy and fast to obtain with a 3D-printer.

The *gyroid* has been selected as the scaffold structure embedded in the paraffin to produce the so called armored grain. In fact, the gyroid is an open cell, easy to print and a triply periodical minimal surface, so a surface that locally minimizes its area [14]. Its triply periodic nature makes it feature an uniform geometry, minimizing the anisotropy in the mechanical properties and avoiding stress concentrations. Gyroid surface is described by Eq. (4) [15].

$$\sin\left(\frac{2\pi x}{L}\right)\cos\left(\frac{2\pi y}{L}\right) + \sin\left(\frac{2\pi y}{L}\right)\cos\left(\frac{2\pi z}{L}\right) + \sin\left(\frac{2\pi z}{L}\right)\cos\left(\frac{2\pi x}{L}\right) = 0 \tag{4}$$

In Eq. (4), L is the cubic unit cell edge length. The gyroid cell obtained using Eq. (4) can be seen in Fig. 1. A thickness d is associated to the gyroid surface to create the solid lattice.
The gyroid lattice is generally produced by additive manufacturing because of its complex geometry. Yan et al. [16] fabricated gyroid lattice of 15% volume fraction (also called volumetric infill) using the selective laser melting (SLM) process. Qin et al. [17] investigated 3D graphene assemblies shaped as gyroids. They also printed and tested 3D gyroid models in VeroMagenta. The mechanical scaling laws identified for graphene agree with the ones for VeroMagenta.

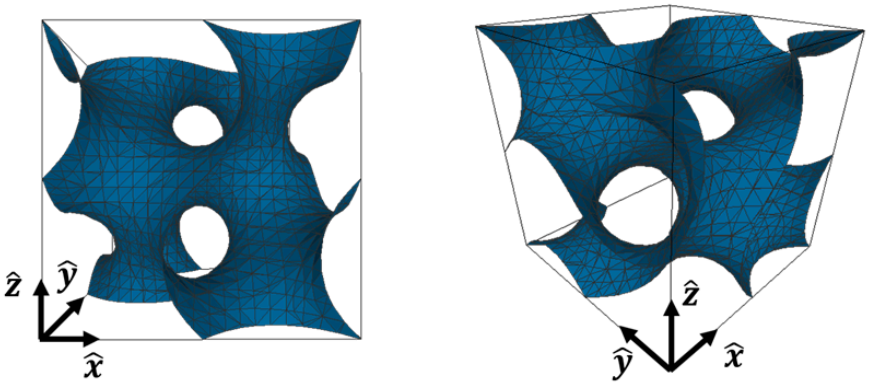

Figure 1: Different views of a gyroid cell.

3. Investigated Materials

In the study, fuel formulations based on a commercial microcrystalline paraffin wax (SasolWax 0907) are considered. The two different approaches of reinforcing paraffin solid fuels result in two groups of investigated fuels grain: **paraffin-based blends** and **armored grains**. All the fuel formulations are loaded with 1 wt% carbon black (CB). The paraffin-based blends use styrene-ethylene-butylenestyrene grafted with maleic anhydride copolymer (SEBS-MA) as reinforcing agent. The armored grains consists in SasolWax 0907 and the 3D-printed gyroid structure embedded in the paraffin wax. Three different thermoplastic polymers has been used to build the gyroid cellular structure: polylactic acid (PLA), Acrylonitrile Butadiene Styrene (ABS), nylon (NY).

3.1 Solid Fuel Components

Paraffin Wax. A microcrystalline paraffin wax (SasolWax 0907) supplied by Sasol GmbH is investigated. This solid paraffin is characterized by higher thermal stability compared to common macrocrystalline waxes. SasolWax 0907 has an average chemical composition of $C_{50}H_{102}$, the congealing point is 83-94 °C, while the density is 0.924 g/cm^3 [18].

Maleic Anhydride Grafted SEBS. Maleic anhydride grafted SEBS is provided by Sigma-Aldrich. It a commercial thermoplastic copolymer characterized by high mechanical and thermal properties. The central ethylene-butylene block is responsible for the rubber-like consistency of the material, styrene monomers confer to SEBS its thermopolastic behavior [6] . The copolymer features a melting temperature of 182-187 °C and a density of 0.910 g/cm^3.

Carbon Black. All paraffin-based formulations have been filled with carbon powder provided by SigmaAldrich (density 2.1 g/cm^3). This is done to enhance radiative heat transfer from flame to the fuel surface and to prevent too deep thermal penetration into bulk fuel, that would result in reduced mechanical strength.

Polylactic acid (PLA). The polylactic acid (PLA) is a biodegradable thermoplastic aliphatic polyester, derived from renewable biomass. For that reason, PLA can be considered a *green material*. The PLA is widely used in FDM because it is easy to print and cheap. The stress-strain curve of PLA is depicted in Fig. 2, where a post-yield softening can be appreciated.

Acrylonitrile Butadiene Styrene (ABS). The Acrylonitrile Butadiene Styrene (ABS) is a thermoplastic polymer. Thanks to its good mechanical and thermal properties it is commonly employed in FDM, though warping is a troublesome problem during the printing. The stress-strain curve is plotted in Fig. 2. Compared to PLA, ABS has a lower Young modulus and yield stress. However, ABS features a higher yield strain and a nearly constant post-yield stress.

Nylon (NY). Nylon possesses a good thermal resistance and is characterized by toughness. It absorbs a moderate quantitative of energy during the deformation, as visible in Fig. 2. This behavior complicates the identification of the yield point, i.e. *first stress at which an increase in strain occurs without an increase of stress* (refer to ISO 604 standard [19]). According to ISO 13314 [20] the compression 0.2% offset stress was used as alternative to the yield strength.

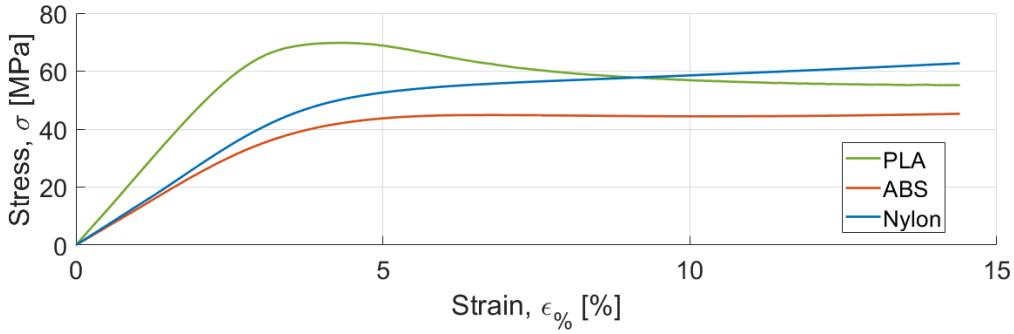

Figure 2: Engineering stress-strain curves: PLA, ABS, nylon compression behavior. Note: the curves are average curves, numerically derived by four runs for each material tested.

3.2 Paraffin-based Fuels

The investigated paraffin-based fuel blends are listed in Table 1, where the detailed compositions and the viscosities are reported.

3.3 Armored Grain

The investigated gyroid lattice structures and the armored grains are reported in Table 2. Polylactic acid (PLA) has been selected for the gyroid characterization because of it ease to print and its eco-friendliness. The experimental campaign consists in two steps: the assessment of the gyroid structure alone and the investigation of the armored grain as a new reinforced paraffin-based fuel. The tested specimens are reported in Table 2. Three different gyroids featuring 7%,

Table 1: Investigated formulations: paraffin-based fuels.

Fuel ID	Ingredients, wt % SasolWax 0907	SEBS-MA	CB	Dynamic viscosity[a], η [Pa·s]
W1	99	0	1	0.005[b]
S05W1	94	5	1	0.014 ± 0.001
S10W1	89	10	1	0.040 ± NAv.

[a]Shear rate 1000 s^{-1}, T=150 °C
[b]For W1, over three measurements, the confidence interval is < 0.001

10%, 15% relative density $\tilde{\rho}$ [1] were tested (refer to samples named PLA_iXX in Table 2). Those gyroid structures were used as the embedded reinforcement for SasolWax 0907, producing the so called "armored grains" (refer to samples named W1_PLA_iXX in Table 2). Nylon and ABS armored grains were also studies for the 15% infill to inspect the effect of different polymers with the same reinforcement structure.

Table 2: Investigated formulations: gyroid structures (no W1) and armored grains (gyroid + W1).

Specimen ID	Gyroid material	Infill	W1
PLA_i07	PLA	7%	NO
PLA_i10	PLA	10%	NO
PLA_i15	PLA	15%	NO
W1_PLA_i07	PLA	7%	YES
W1_PLA_i10	PLA	10%	YES
W1_PLA_i15	PLA	15%	YES
W1_ABS_i15	ABS	15%	YES
W1_NY_i15	Nylon	15%	YES

4. Procedures and Methods

The characterization and comparison between the two paraffin grains reinforcement strategies (paraffin-based blend and armored grain) were pursued through different steps. Firstly, the production of gyroid lattice was addressed along with the manufacturing process of both paraffin blends and armored grains. Secondly, thermogravimetric analysis and materials compatibility were performed to characterize the raw components of the fuels. Lastly, the structural behavior of paraffin blends and armored grains was addressed by means of compression tests.

4.1 Gyroid Production Methodology

The gyroids were printed by means of a commercial FDM 3D-printer, exploiting two different methods.
The first one consisted in the following steps:

1. A digital 3D-model of the object was prepared.
2. The model was converted into a .STL file, turning the surface into a triangular mesh.
3. The .STL was processed by a software called *slicer* creating the .G-code file, containing a series of instructions for the printer. The model was printed.

The infill is the structure that *fills* any additive manufactured object. The infill is characterized by its density, expressed in percentage, and its pattern, e.g. grid, concentric, honeycomb. A 0% infill produces a cave object, while a 100% infill is equivalent to a solid print. In the present work, infill density (or volumetric infill) coincides with the relative density $\tilde{\rho}$. Prusa releases also a customized version of the Slic3r slicer provided with a gyroid infill pattern. For that reason, the gyroid for the armored grain is easily printable: given the shape and the size of the final cylindrical grain (30 mm diameter, 50 mm height), entering the slicer settings, it is possible to remove the perimeters and to print only the infill.

[1] In the present paper relative density $\tilde{\rho}$ is also named volumetric infill or infill density

The 3D-printed gyroids features a strut thickness d that is equal to the extrusion width, hence $d = 0.45$ mm.
This method allows an easy gyroids production with the specified relative density, since a CAD file of a cylinder is simply required. For the sake of clarity, the gyroid generated with this procedure are called *infill gyroid*.

The second method consisted in the following step:

1. The gyroid *isosurface* described by Eq. (4) was generated.
2. The surface was thickened using MeshLab and the solid gyroid created. Thickness was selected to be 0.45 mm to be consistent with the previous method.
3. The .STL was processed by the *slicer*, creating the .G-code file and, hence, the printed object.

The output of the .STL is a gyroid solid (not a cylinder as in the previous case). For that reason, this file is sent to Slic3r for the slicing. No infill is necessary since the strut width is the same of the extrusion width.
This process produces gyroids with the specified cubic unit cell edge length L (refer to Eq. (4)). For the sake of clarity, the gyroid generated with this procedure is called *SPLab gyroid*.
Extracting the .G-code files obtained for the *infill gyroid* at different relative density (infill), it was possible to retrieve a correlation between L and the relative densities. A perfect match between *infill gyroid* and *SPLab gyroid* was achieved from the geometrical point of view. *Infill gyroid* approach has been selected as the gyroid manufacturing procedure for the armored grains. In fact, *infill gyroid* are optimized for the 3D-printing (flaws and defects are minimized since the gyroid patter is already implemented in the Slic3r) and the printing time is shorter than the *SPLab gyroid*.

4.2 Fuel Grains Manufacturing

In order to perform mechanical tests, the paraffin blends and the armored grains needed to be shaped into cylindrical specimens of 30 mm diameter and 50 mm height. The dimensions are compliant with the standard employed in ISO 604 [19] and in combustion runs performed at SPLab (refer to [21]). In both cases, the paraffin wax had to be fully melted and poured into a cylindrical mold. The wax pouring process could produce voids in the grain due to the inherent volumetric shrinkage of wax of about 15 - 25% [22]. Constant pressure shall be applied during the cooling process to prevent flaws in the fuel grain. The reinforced paraffin-based fuels were obtained by blending paraffin wax with SEBS-MA (5% and 10% mass fraction) via casting approach. A casting procedure was also exploited for the armored grains production. Firstly, the 3D-printed gyroid structure was inserted in a specific case. Secondly, the melted paraffin was poured into the mold. Constant pressure was applied during the cooling process for both paraffin-based blends and the armored grains. All the specimens were finally turned and refined to ensure the shape accuracy and surface finishing as prescribed by ISO 604 [19].

4.3 Simultaneous Thermal Analysis (TGA/DSC)

Thermogravimetric analysis (TGA) was performed simultaneously with differential scanning calorimetry (DSC) to obtain information about the response of materials to thermal inputs. The investigated materials were the paraffin-based fuels (Table 1) and the 3D-printer polymers (PLA, ABS, nylon). Thermal analyses were carried out with a Netzsch STA 449 F5 Jupiter with vertical weighting system. Tests were performed on 10 mg samples (nominal mass) under argon flow. The temperature range was 25-800 °C with an heating rate of 10 °C/min. Degradation onset and end temperatures were evaluated with the tangent method. An example of onset T_{on} and end T_{end} temperature determination can be seen in Fig. 3, where the TGA (solid line) and DSC (dashed line) of PLA are reported. As shown Fig. 3, the DSC measurement is useful to retrieve information about the glass transition temperature T_g, the melting temperature T_m (peak temperature) and the heat of fusion.

4.4 Materials Compatibility and Wettability

Polymers and SasolWax compatibility and wettability were studied measuring the critical surface tension γ_c, the surface free energy (of a solid) γ and its polar γ^p and dispersion γ^d components.
Wettability investigation is crucial for the armored grain manufacturing since it is produced by casting the melted paraffin. For that reason, good adhesion between 3D-printer material and paraffin is needed. Critical surface tension is defined as the surface tension at which a liquid completely wets the solid. According to Fox-Zisman method [23] an empirical rectilinear relation was found between the cosine of the liquid-solid contact angle ($\cos(\theta)$) and the surface tension of a series of testing liquids. The intercept of the line at $\cos(\theta) = 1$ is the critical surface tension γ_c. A low critical surface tension means that the surface is more prone to be wetted by a liquid.

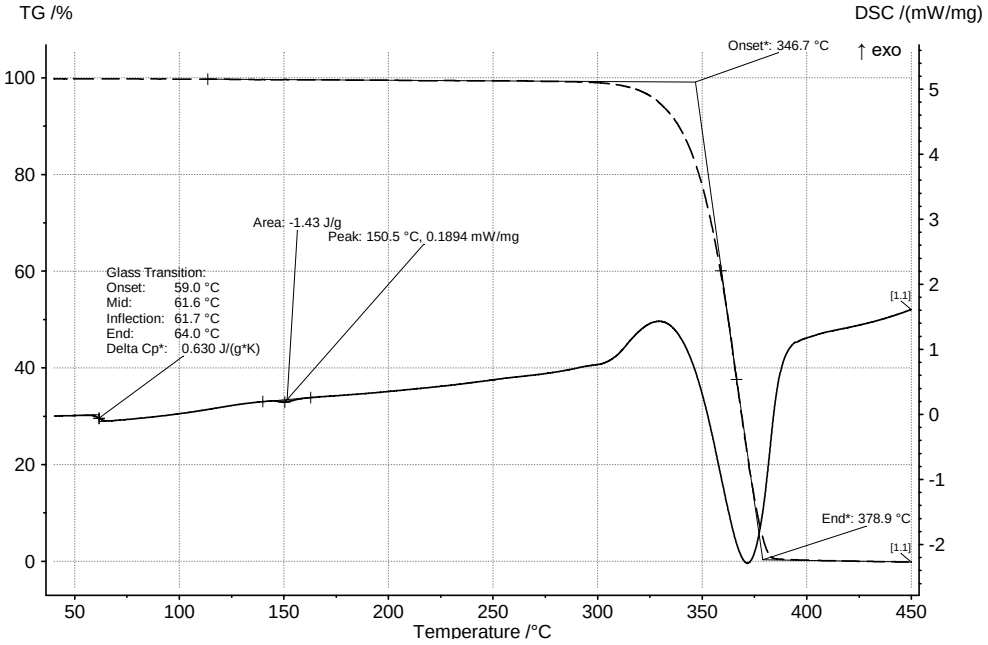

Figure 3: Thermogravimetry analysis TGA (solid line) and differential scanning calorimetry DSC (dashed line) of PLA. Heating rate of 10 °C/min, 10 mg sample mass, Ar atmosphere.

Surface free energy and polarity of the 3D-printer polymers and the SasolWax were calculated according to the Owens-Wendt method [24]. This method uses the contact angles of two testing liquids and the following equations.

$$(1 + cos(\theta_1))\,\gamma_1 = 2\left(\gamma_1^d\,\gamma_s^d\right)^{1/2} + 2\left(\gamma_1^p\,\gamma_s^p\right)^{1/2} \tag{5}$$

$$(1 + cos(\theta_2))\,\gamma_2 = 2\left(\gamma_2^d\,\gamma_s^d\right)^{1/2} + 2\left(\gamma_2^p\,\gamma_s^p\right)^{1/2} \tag{6}$$

In Eqs. (5) and (6), $\gamma = \gamma^p + \gamma^d$ and the subscripts 1, 2 and s refer respectively to the testing liquid 1 and 2, and to the investigated polymer at the solid state. Water and methylene iodine are two convenient testing liquids, whose γ^p and γ^d values are available in open literature [25]. Equations (5) and (6) can be solved through algebraic manipulations (refer to Appendix I in [25]) to retrieve γ_s^d and γ_s^p . The measurement of the solids surface tension provides an overview of the adhesion between SasolWax 0907 and the gyroids printed with the three different polymers (PLA, ABS, NY). The ideal reversible work of adhesion W_a is defined as the free energy change required to separate the two phases. The work of adhesion W_a between two bulk phases α and β can be evaluated by means of Eq. (7) [24]:

$$W_a = W_a^d + W_a^p = 2\left(\gamma_\alpha^d\,\gamma_\beta^d\right)^{1/2} + 2\left(\gamma_\alpha^p\,\gamma_\beta^p\right)^{1/2} \tag{7}$$

where the superscripts d and p, refer respectively to the dispersion and polar component, γ_α is the surface tension of phase α, γ_β the surface tension of phase β. Contact angles were determined via sessile method [25]. Measurements were performed on 3D-printed plates of the three different 3D-printer materials. The plates were smoothed using a press to reduce surface roughness, hysteresis and capillarity penetration phenomena, affecting the results reliability.

4.5 Mechanical Characterization

Uniaxial compression tests were conducted on paraffin grains, 3D-printed bulk grains, gyroid lattices and armored grains. All tests were carried out at a speed of 1 mm/min at ambient temperature. At least four samples for each type of specimen were tested. The adopted standard for plastics compression properties is ISO 604 [19]. The standard does not impose specific specimen size and shape. Therefore, the specimen was cylindrically shaped and sized according to the standard employed in combustion runs (see [21]). The dimensions are 30 mm diameter and 50 mm height. Taking into account the sample size, results can be considered valid until a maximum strain of 14.4% is reached. Above this value, the specimen could undergo buckling [19]. The test campaign was conducted on a MTS 810 universal testing machine equipped with a 250 kN load cell.

5. Results and Discussion

5.1 Paraffin and Paraffin-based Blends

The manufacturing process could affect both the mechanical and thermal behavior of paraffin fuels. For that reason, the TGA-DSC measurements of the pure wax (W1) and the two blends (S05W1 and S10W1) were performed without providing any preliminary heating-cooling run. This was done to prevent any possible effect of cooling rate on the the paraffin crystal structure. Results are reported in Table 3. DSC scanning detected two endothermic peaks for paraffin wax blends S05W1 and S10W. The first one is related to the pre-melting solid-solid crystalline transition T_1 and the second to solid phase melting T_2. On the contrary, pure paraffin (W1) experienced only one peak temperature.
An increase in SEBS-MA mass fraction in the paraffin-based fuels was observed to cause also a rise in degradation onset temperature T_{on} and a reduction of the degradation end temperature T_{end}.

Table 3: Thermal parameters obtained from TGA-DSC measurements of paraffin-based blends W1, S05W1, S10W1. Heating rate of 10 °C/min, 10 mg sample mass, Ar atmosphere.

Specimen	**First peak temperature**[a], T_1 [°C]	**Second peak temperature**[b], T_2 [°C]	**Degradation Onset temperature**, T_{on} [°C]	**Degradation End temperature** T_{end} [°C]
W1	-	73.1	329.2	485.4
S05W1	66.2	86.2	361.7	472.7
S10W1	64.1	81.1	373.3	461.7

[a]It coincides with the temperature associated to the pre-melting solid-solid crystalline transition.
[b]It coincides with the temperature associated to the endothermic melting peak.

Compression tests were performed to determine the mechanical properties of paraffin blends and to quantify the strengthening effect of SEBS-MA addition to the pure paraffin (W1). The results are reported in Table 4. Addition of SEBS-MA makes the pure paraffin wax stiffer and stronger than the unloaded paraffin. In fact, a 5% mass fraction of SEBS-MA increases the Young modulus of 22% and the yield stress of 25%. The same quantities can be respectively increased by 28% and 38% if a 10 wt% of SEBS-MA is added. On the other hand, yield strain is not significantly affected by the presence of the thermoplastic copolymer in the formulation.

Table 4: Mechanical properties of paraffin-based fuel blends.

Specimen	**Young modulus**, E [MPa]	**Yield stress**, σ_y [MPa]	**Yield strain** ϵ_y [%]
W1	407	3.5	1.5
S05W1	497	4.3	1.2
S10W1	519	4.8	1.8

5.2 3D-Printer Materials

The characterization of the 3D-printer materials involved their thermal and wettability investigation. The thermal behavior is reported in Table 5. The analysis highlighted the amorphous nature of ABS because of the absence of a melting temperature. All the polymers feature a glass transition temperature. The low glass transition temperature of PLA makes it less attractive for high temperature applications with respect to ABS. However, this could not be a detrimental aspect since the gyroid polymer structure is supposed to burn with the paraffin, whose melting point is below 100 °C (refer to Table 3). The evaluation of the degradation onset and end temperature suggests that nylon is the most stable material from the thermal view point. On the contrary, PLA is the polymer that degrades at the lowest temperature. Its degradation onset temperature is only 20 °C higher than the W1 paraffin fuel (refer to Table 3). All polymers feature a degradation end temperature slightly lower than the one of W1 fuel, reducing the possibility of an irregular combustion of the two main components in the armored grain (i.e., the polymer gyroid structure and the paraffin).

The gyroid structure embedded in the paraffin fuel grain is aimed at providing mechanical strength. To achieve this goal, the most appealing material from the mechanical point of view should be selected. At the same time,

Table 5: Thermal parameters obtained from TGA-DSC measurements of PLA, ABS, NY. Heating rate of 10 °C/min, 10 mg sample mass, Ar atmosphere.

Specimen	**Glass transition temperature,** T_g [°C]	**Melting temperature**[a]**,** T_m [°C]	**Degradation Onset temperature,** T_{on} [°C]	**Degradation End temperature,** T_{end} [°C]
PLA	61.7	150.5	346.7	378.9
ABS	110.1	-	374.3	452.6
NY	56.6	191.1	423.0	471.6

[a]It coincides with the temperature associated to the endothermic melting peak.

it is also important to study the adhesion between the gyroid material and the paraffin. Since the manufacturing procedure for the armored grain is based on the casting procedure of liquid paraffin, the wettability of polymers has to be addressed. The critical surface tension results for the PLA, ABS and nylon are reported in Fig. 4. Polymers are low-energy surfaces and the critical tensions for the three investigated material are close to each other. Materials with higher critical tension should be preferred since this is the upper threshold for a liquid to wet completely the solid. In particular, the liquid is the SasolWax 0907 during the manufacturing of the armored grain. Its surface tension at 110 °C is 27.5 mN/m [26]. This value is below the critical tension of all the investigated polymers. It can be stated that the liquid paraffin completely wets all polymers. This aspect is important for the armored grain manufacturing. However, it should be pointed out that the roughness of the 3D-printing process could obstacle the paraffin-polymer wetting. Concerning the wettability, PLA and nylon seems to be the most promising materials.

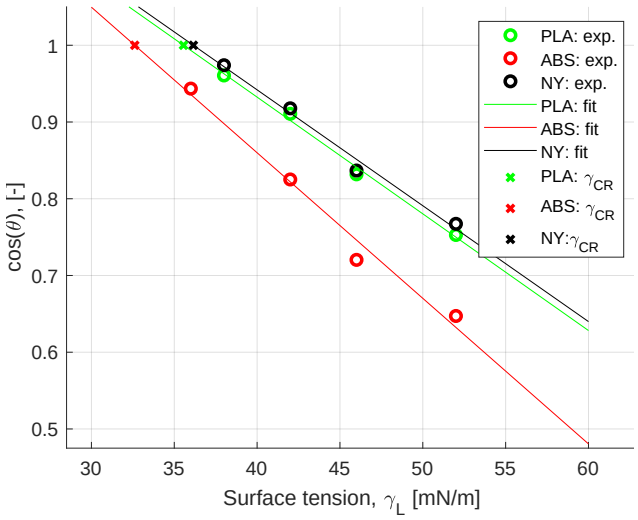

Figure 4: Contact angles and critical surface tension of 3D-printer polymers. For the sake of clarity, error bars and 95% confidence interval of the fittings are not reported.

5.3 Gyroid Structure Behavior

The mechanical assessment of the empty gyroid structures was performed by means of compression tests (refer to Section 4.5). They were carried out on three different relative densities $\tilde{\rho}$. The nominal values are 7%, 10%, 15%. For the sake of completeness, the tested gyroids were produced following both the production methodologies explained in Section 4.1. The mechanical behavior of the infill gyroids (PLA_iXX) can be appreciated in Table 6, while in Table 7 the SPLab gyroids (SPLA_iXX) characterization is reported. The tables highlight a connection between higher relative densities and higher mechanical properties, in terms of stiffness, strength, and elastic limit enhancement. Data suggest a similar behavior of infill gyroids and SPLab gyroids. However, the yield strain of PLA_i15 differs from the one of SPLA_i15. The reason for the high yield strain of SPLA_i15 is that its stress-strain curve features a stress hardening and it does not experience a drop after the elastic limit. It should be also pointed out that the actual relative densities of infill gyroids and SPLab gyroids are slightly different. In fact, different gyroid production techniques affect the printing

process, in turn responsible for the presence of flaws and open saddle points.

Table 6: Mechanical properties of PLA Infill gyroids.

Specimen	**Young modulus**, E [MPa]	**Yield stress**, σ_y [MPa]	**Yield strain**, ϵ_y [%]	**Lattice density**, ρ [g/cm^3]	**Relative density**, $\tilde{\rho}_{\%}$ [%]
PLA_i07	31	0.7	2.5	0.09	7.8
PLA_i10	60	1.5	3.1	0.12	10.2
PLA_i15	109	3.0	3.9	0.17	14.6

Table 7: Mechanical properties of PLA SPLab gyroids.

Specimen	**Young modulus**, E [MPa]	**Yield stress**, σ_y [MPa]	**Yield strain**, ϵ_y [%]	**Lattice density**, ρ [g/cm^3]	**Relative density**, $\tilde{\rho}_{\%}$ [%]
SPLA_i07	36	0.8	2.7	0.10	8.4
SPLA_i10	66	1.9	3.4	0.14	11.8
SPLA_i15	88	3.1	6.2	0.21	17.5

Experimental test campaign highlights that higher relative density $\tilde{\rho}$ results into better mechanical properties. According to [12], the Young modulus varies as

$$\frac{E}{E_s} = a_E \cdot \tilde{\rho}^{\,n_E} \tag{8}$$

For what concerns the yield stress, the strut slenderness and the experiments suggested a buckling collapse mechanism of the investigated structures. For this reason, the employed yield stress law is:

$$\frac{\sigma_y}{E_s} = a_\sigma \cdot \tilde{\rho}^{\,n_\sigma} \tag{9}$$

The application of Eqs. (8) and (9) requires the Young modulus of the bulk material (refer to Fig. 2). The results from compression tests are represented in Figs. 5a and 5b, respectively showing the Young modulus and the yield stress trend versus relatives density. For the sake of generality, one mathematical fit was proposed for the experimental results, considering both the infill gyroids and the SPLab gyroids. It can be noted that the experimental results for infill gyroids and SPLab gyroids become closer in terms of mechanical properties and relative density for lower infills. The experimental fitting curve matches quite well the infill gyroids and SPLab gyroids data. This evidence is valid considering both the Young modulus (Fig. 5a) and the yield stress (Fig. 5b).

The fitting curves coefficients are reported in Table 8 for the Young modulus and in Table 9 for the yield stress. The coefficients predicted by Ahsby [12] are also shown in addition to the experimental results. Focusing on the pre-exponential factors, the same order of magnitude is recorded. In particular, the experimental and numerical a_E values coincide with the theoretical one. The exponential factors n_E for the Young modulus scaling law is closer to 2 rather then to 1, suggesting that gyroid lattice deforms in a bending-dominated manner.

Table 8: Young modulus scaling laws coefficients for experimental test.

Young modulus scaling law (Eq. (8)) coefficients	a_E	n_E	R^2_{Adj}
Ashby [12] **bending-dominated**	1	2	-
Ashby [12] **stretching-dominated**	1	1	-
PLA gyroids	1.00	1.72	0.9996

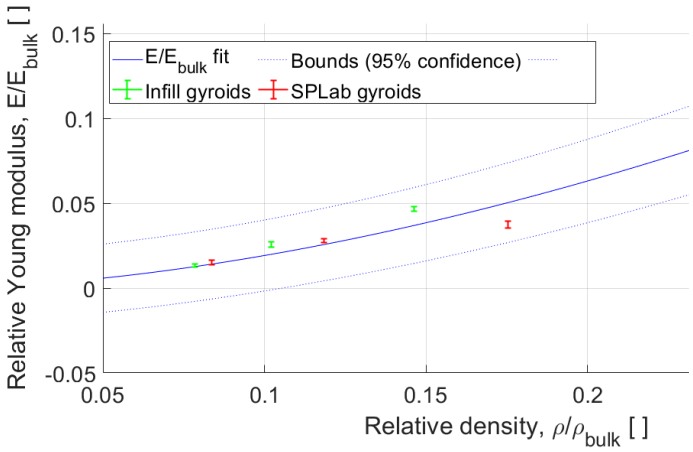

(a) Gyroid relative Young modulus vs. relative density

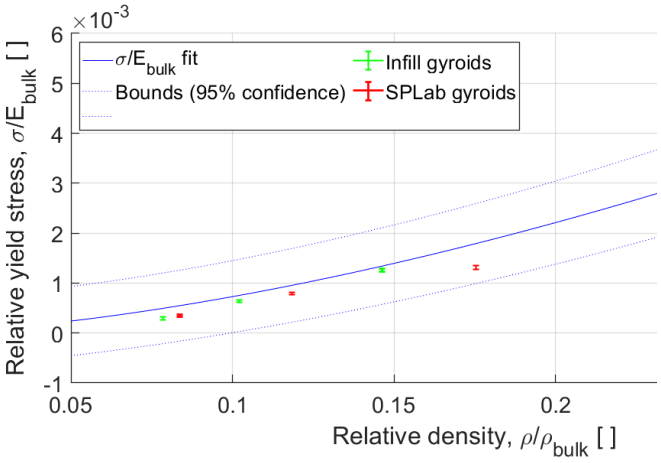

(b) Gyroid relative yield stress vs. relative density

Figure 5: Young modulus scaling law (Eq. (8)) and yield stress scaling law (Eq. (9)) vs. relative density for PLA gyroids.

Table 9: Yield stress scaling laws coefficients for experimental test.

Yield stress scaling law (Eq. (9)) coefficients			
	a_σ	n_σ	R^2_{Adj}
Ashby [12]	0.05	2	-
PLA gyroids	0.03	1.60	0.9999

5.4 Armored Grain

The armored grain investigation is essentially based on experimental compression tests. However, a preliminary study about paraffin-polymer adhesion was carried out. The wettability results attested that paraffin in the liquid state should wet completely all the polymers, hence the gyroid structure, regardless the material it is made of. The adhesion of gyroid structure and paraffin was studied by measuring the materials surface free energy and the reversible ideal work between paraffin (W1) and each polymer. The results are reported in Table 10. The surface free energy of polymers is mainly affected by the dispersion component. Among all the polymers, the one that features the highest polar component is the PLA. On the contrary, the polar contribution in paraffin (W1) can be considered negligible. Considering the work of adhesion, no significant difference between polymers can be appreciated. From the adhesion point of view, all polymers are suitable to be the 3D-printer material for the gyroid.

The mechanical properties of armored grains were investigated for PLA exploiting three different infill (7%, 10%

Table 10: Surface free energy of investigated material and work of adhesion paraffin-polymer.

Specimen	**Surface free energy = polar + dispersion** $\gamma = \gamma^p + \gamma^d$ [mJ/m^2]	**Work of adhesion W1-polymer,** W_a [mJ/m^2]
W1	0.4 + 37.3 = 37.67	-
PLA	15.4 + 36.8 = 52.2	79.0
ABS	9.9 + 37.0 = 46.9	78.3
NY	10.4 + 36.4 = 46.8	77.8

and 15%), and for ABS and nylon at 15% infill. A typical compression run is shown in Fig. 6, where it can be noted the formation of small paraffin scales but no crack occurrence. The mechanical behavior of the armored grains can be appreciated in Fig. 7. The figure shows the ductility achieved thanks to the armored grains reinforcement gyroid structure. While W1 features a significant after-yield stress decrease, the addition of the PLA gyroids stops this decay to a plateau value, whereas ABS and nylon are characterized by a plastic stress of the same order of the yield stress. Actually, the insertion of a gyroid reinforcement structure in the paraffin affects the mechanical properties of pure paraffin W1 as follows:

- **Young modulus**. The Young modulus of armored grains is generally lower, or at least of the same order, than that of pure paraffin. This is not a critical point since the Young modulus of pure paraffin is about two order of magnitude higher than the ones of a common HTPB-based propellant.
- **Compressive yield stress and strain**. The yield stress augments with a $\tilde{\rho}$ enhancement and depends on the material. The same applies for the yield strain.
- **Ductile material**. The brittle behavior of paraffin is definitely changed into ductile. This may be of great interest since it extends the strain before rupture and augments the deformation energy that the grain can absorb. This is the the real breakthrough of the armored grain concept.

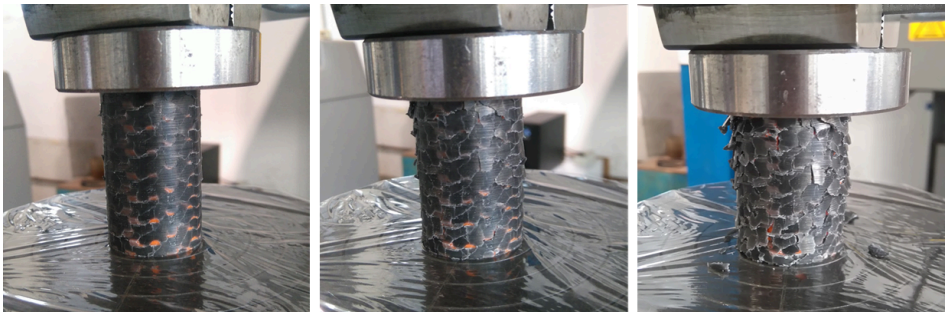

Figure 6: Pictures of W1_ABS_i15 during the compression test.

6. Conclusions

The armored grain, a paraffin grain reinforced with a 3D-printed cellular structure, was investigated and proposed as a solution to cope with the fragility of paraffin fuels. The selected cellular structure was the gyroid, a triply periodical minimal surface that can be easily 3D-printed. A complete pre-burning and mechanical characterization of the armored grain was performed. Three different reinforcement materials were employed: polylactic acid (PLA), Acrylonitrile Butadiene Styrene (ABS) and nylon (NY). The mechanical properties and the thermal behavior of the bulk materials were studied by means of compression tests and thermal analyses. Materials compatibility investigation was also carried out to understand if the different polymer-paraffin (W1) couples could satisfy the wetting and adhesion criteria. Satisfying results were achieved for all the 3D-printer materials. Characterization of the gyroid was performed via compression tests on PLA gyroids featuring different relative densities. It was observed that the compressive yield stress and strain are monotonically enhanced by the presence of denser lattices. The achieved results were useful to understand the behavior of gyroid mechanical properties and to capture their scaling laws. Eventually, the effectiveness of the armored grain was assessed by inspecting the mechanical performance. Armored grains featuring different gyroid structures and material (PLA, ABS, nylon) were studied via compression tests. The results highlighted an

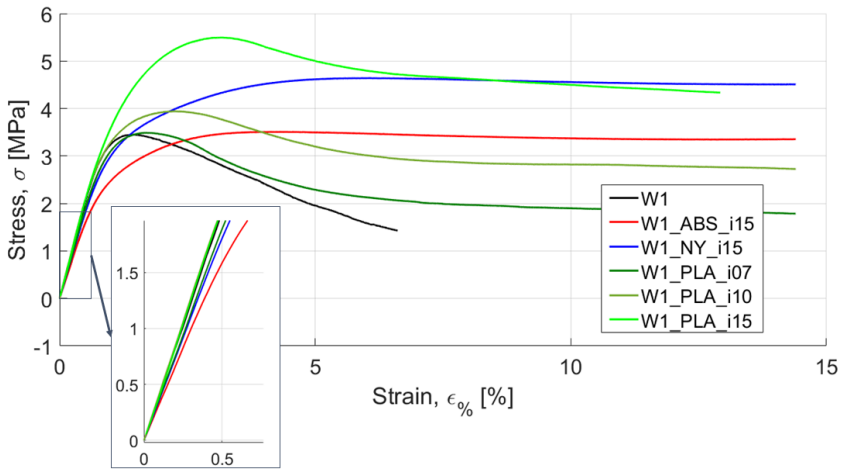

Figure 7: Engineering stress-strain curves comparison: armored grains vs W1. Note: the curves are average curves, numerically derived by four runs for each sample tested.

enhancement of the compression yield stress and strain with respect to the pure paraffin (W1). The most significant increments were achieved with the denser gyroids made of PLA. Considering the mechanical properties, the armored grain strategy revealed to be more effective than the traditional approach of blending paraffin with polymers. In fact, the armored grain mechanical behavior is ductile rather than fragile. This is the most dramatic effect of reinforcing fuels with embedded gyroids, instead of blending paraffin with polymers. The present work offers an overview of this new approach potentialities, paving the way for a new generation of high-performance green paraffin-based fuels.

References

[1] D. Altman, "Overview and history of hybrid rocket propulsion," in *Fundamentals of Hybrid Rocket Combustion and Propulsion* (M. J. Chiaverini and K. K. Kuo, eds.), ch. 1, pp. 1–36, American Institute of Aeronautics and Astronautics, 2007.

[2] M. A. Karabeyoglu, G. Zilliac, B. J. Cantwell, S. DeZilwa, and P. Castellucci, "Scale-up tests of high regression rate paraffin-based hybrid rocket fuels," *Journal of Propulsion and Power*, vol. 20, no. 6, pp. 1037–1045, 2004.

[3] C. Paravan, R. Bisin, S. Carlotti, F. Maggi, and L. Galfetti, "Diagnostics for Entrainment Characterization in Liquefying Fuel Formulations," *54st AIAA/SAE/ASEE Joint Propulsion Conference*, no. AIAA 2018-4830, pp. 1–12, 2018.

[4] M. Kobald, C. Schmierer, H. Ciezki, S. Schlechtriem, E. Toson, and L. T. De Luca, "Evaluation of Paraffin-based Fuels for Hybrid Rocket Engines," *50th AIAA/ASME/SAE/ASEE Joint Propulsion Conference*, no. AIAA 2014-3646, pp. 1–14, 2014.

[5] S. Kim, H. Moon, J. Kim, and J. Cho, "Evaluation of Paraffin polyethylene Blends as Novel Solid Fuel for Hybrid Rockets," *Journal of Propulsion and Power*, vol. 31, no. 6, pp. 1750–1760, 2015.

[6] C. Paravan, L. Galfetti, and F. Maggi, "A Critical Analysis of Paraffin-based Fuel Formulations for Hybrid Rocket Propulsion," *53rd AIAA/SAE/ASEE Joint Propulsion Conference*, no. July, 2017.

[7] L. Galfetti, L. Merotto, M. Boiocchi, F. Maggi, and L. T. DeLuca, "Experimental investigation of paraffin-based fuels for hybrid rocket propulsion," *Progress in Propulsion Physics*, vol. 4, pp. 59–74, 2013.

[8] S. Ryu, S. Han, J. Kim, H. Moon, J. Kim, and S. W. Ko, "Tensile and compressive strength characteristics of aluminized paraffin wax fuel for various particle size and contents," *Journal of the Korean Society of Propulsion Engineers*, vol. 20, no. 5, pp. 70–76, 2016.

[9] S. A. Whitmore, Z. W. Peterson, and S. D. Eilers, "Comparing Hydroxyl Terminated Polybutadiene and Acrylonitrile Butadiene Styrene as Hybrid Rocket Fuels," *Journal of Propulsion and Power*, vol. 29, no. 3, pp. 582–592, 2013.

[10] D. Armold, J. E. Boyer, K. Kuo, J. K. Fuller, J. Desain, and T. J. Curtiss, "Test of Hybrid Rocket Fuel Grains with Swirl Patterns Fabricated Using Rapid Prototyping Technology," *49th AIAA/ASME/SAE/ASEE Joint Propulsion Conference*, no. AIAA 2013-4141, pp. 1–14, 2013.

[11] D. M. Armold, J. E. Boyer, B. McKnight, K. Kuo, J. Desain, B. B. Brady, J. Fuller, and T. J. Curtiss, "Testing of Hybrid Rocket Fuel Grains at Elevated Temperatures with Swirl Patterns Fabricated Using Rapid Prototyping Technology," *50th AIAA/ASME/SAE/ASEE Joint Propulsion Conference*, no. AIAA 2014-3754, pp. 1–13, 2014.

[12] M. F. Ashby, "The properties of foams and lattices," *Philosophical Transactions of the Royal Society A: Mathematical, Physical and Engineering Sciences*, vol. 364, no. 1838, pp. 15–30, 2006.

[13] M. Ashby and R. Medalist, "The Mechanical Properties of Cellular Solids," *The Metallurgical Society of AIME*, vol. 14, no. September, pp. 1755–1769, 1983.

[14] A. H. Schoen, "Infinite Periodic Minimal Surface Without Self-Intersections," *NASA Technical Note TN D-5541*, 1970.

[15] M. Wohlgemuth, N. Yufa, J. Hoffman, and E. L. Thomas, "Triply periodic bicontinuous cubic microdomain morphologies by symmetries," *Macromolecules*, vol. 34, no. 17, pp. 6083–6089, 2001.

[16] C. Z. Yan, L. Hao, A. Hussein, and D. Raymont, "Evaluations of cellular lattice structures manufactured using selective laser melting," *International Journal Of Machine Tools & Manufacture*, vol. 62, pp. 32–38, 2012.

[17] Z. Qin, G. S. Jung, M. J. Kang, and M. J. Buehler, "The mechanics and design of a lightweight three-dimensional graphene assembly," *Science Advances*, vol. 3, no. 1, pp. 1–9, 2017.

[18] M. Grosse, "Effect of a diaphragm on performance and fuel regression of a laboratory scale hybrid rocket motor using nitrous oxide and paraffin," *51st AIAA/SAE/ASEE Joint Propulsion Conference*, no. AIAA 2009-5113, pp. 1–8, 2009.

[19] "ISO 604: Plastics - Determination of compressive properties," tech. rep., International Organization for Standardization, 2002.

[20] "ISO 13314: Mechanical testing of metals - Ductility testing - Compression test for porous and cellular metals," tech. rep., International Organization for Standardization, 2011.

[21] R. Bisin, C. Paravan, A. Verga, and L. Galfetti, "An Innovative Strategy for Paraffin-based Fuels Reinforcement: Part II, Ballistic Characterization," *8th European Conference for Aerospace Sciences*, no. EUCASS 2019-728, 2019.

[22] F. Piscitelli, G. Saccone, A. Gianvito, G. Cosentino, and L. Mazzola, "Characterization and manufacturing of a paraffin wax as fuel for hybrid rockets," *Propulsion and Power Research*, vol. 7, no. 3, pp. 218–230, 2018.

[23] H. Fox and W. Zisman, "The spreading of liquids on low energy surfaces. 1. polytetrafluoroethylene," *Journal of Colloid Science*, vol. 5, no. 6, pp. 514–531, 1950.

[24] D. Owens and R. Wendt, "Estimation of the surface free energy of polymers," *Journal of Applied Polymer Science*, vol. 13, pp. 1741–1747, 1969.

[25] S. Wu, *Polymer Interface and Adhesion*. Marcel Dekker Inc., New York, first ed., 1982.

[26] M. Kobald, E. Toson, H. Ciezki, S. Schlechtriem, S. Di Betta, M. Coppola, and L. DeLuca, "Rheological, optical, and ballistic investigations of paraffin-based fuels for hybrid rocket propulsion using a two-dimensional slab-burner," *Progress in Propulsion Physics*, vol. 8, pp. 263–282, 2016.